Design of Flux-Axis Angular Speed Estimation using Induced Voltage in Speed Sensor-less Field Oriented Control for Induction Motor

Jun-ichi Itoh[1], Kazuya Kawai[1], Koroku Nishizawa[1], Hiroki Watanabe[1]
[1] Nagaoka University of Technology, Japan

***Abstract*-- This paper proposes a design method of the flux-axis angular speed estimation using induced voltage in a speed sensor-less field oriented control for induction motor (IM) drive systems. In this method, the d-axis induced voltage is regulated to zero by a feedback control to estimate the flux-axis angular speed. A low pass filter (LPF) is necessary in this estimation to avoid the recursive calculation. In this paper, the design method of compensation gain k_{pem} and the cut-off angular frequency of LPF ω_{lpf} are considered. As a result, the relation between k_{pem}, ω_{lpf}, convergence time of the d-axis induced voltage have a match to the equation and designed model in this paper. Furthermore, the maximum error between the simulation and estimated results of the time constant of the flux-axis angular speed introduced due to LPF is 3.7% when ω_{lpf} is 200 rad/s. As the experimental results, when a torque step of 100% is applied to the induction motor, the convergence time of the motor speed is 1.6 s as the worst case with k_{pem} set as 2.0 p.u. and the cut-off angular frequency set as 1000 rad/s. However, if k_{pem} is set as 2.0 p.u. and ω_{lpf} is set as 400 rad/s, the convergence time of the motor speed is 0.43 s as the best case, which is reduced by 73.1% compared to the worst case. As the result, k_{pem} should decide by the target steady-state error, ω_{lpf} should bigger than the cut-off angular frequency of the PI controller ω_{ASR}. Where, if the ω_{lpf} is high, the convergence time of the motor speed is high.**

***Index Terms*— Induction motor, vector control, sensor-less field oriented control, control design.**

I. Introduction

In recent years, induction motors (IM) are used in many fields due to their low cost and easy maintenance. As a control method for IM, a field oriented control (FOC) is employed for torque control, high speed response, high efficiency, and smooth control in low-speed region. In general, a speed sensor is necessary for the detection of the actual speed. However, the speed sensor limits cost reduction of the motor drive systems. On the other hand, a sensor-less FOC overcomes this problem by the achievement of the torque control performance close to the sensor-equipped FOC without speed sensors. The sensor-less FOC is accomplished by the implementation of speed estimation methods in the feedback control [1-19]. One of the sensor-less FOC methods is a model reference adaptive system (MRAS). MRAS is based on the observer and the adaptive control to calculate flux-axis angular speed. This method uses both the voltage and current models [14-20]. Besides, the convergence speed of the estimation rule is slowly [20]. Furthermore, the induced voltage and secondary flux are used in order to calculate the flux-axis angular speed, resulting a simpler algorithm than other sensor-less FOC methods [6-13]. However, the design method of the flux-axis angular-speed estimation using the induced voltage, the compensation gain and the low pass filter (LPF), has not been clarified [6-9].

This paper proposes the design method of the flux-axis angular-speed estimation using the induced voltage. The closed transfer function of the flux-axis angular-speed estimation with LPF is derived to evaluate the control performance of the d-axis induced voltage regulator. The originality of this paper is that the clarification of the relation between the compensation gain and LPF in the flux-axis angular-speed estimation, which ensures the stable operation of the speed sensor-less FOC. As a result, the estimated value of the d-axis induced voltage has a match to the actual value. Furthermore, the maximum error between the simulation and estimated results of the time constant of the flux-axis angular speed introduced by LPF is 3.7% when the cut-off angular frequency of LPF ω_{lpf} is 200 rad/s. As experimental results, it is confirmed the convergence time of the motor speed error is reduced by 73.1% in a torque step is applied.

This paper is organized as follows; in section II, the sensor-less FOC using the induced voltage to estimate flux-axis angular-speed is introduced with the past studies. The transfer function of the flux-axis angular-speed estimation and the design method for k_{pem} and ω_{lpf} are explained as the main part of this paper in the section III. Next in the section IV, the simulation with IM model is carried out to confirm the validation of the transfer function of the flux-axis angular-speed estimation, which shows the relation between the compensation gain, the cut-off frequency of LPF and the convergence time of the flux axis angular speed. Finally, in section V, the design method for k_{pem} and ω_{lpf} is confirmed by the experiments.

II. Control Method and Principle of Flus-axis Angular Speed Estimation

A. Configuration of Speed Sensor-less Controller

Fig. 1 shows the control block diagram of the speed sensor-less FOC using the induced voltage. Note that ω_r^*

is the rotor angular speed, $\hat{\omega}_r$ is the calculated rotor angular speed, ω_s is the slip angular speed, i_d^* and i_q^* are the currents command on dq-axis, i_d and i_q are the currents on dq-axis, e_d and e_q are the dq-axis induced voltages, v_u^*, v_v^*, v_w^* and i_u, i_u, i_w are the of output voltages command and the motor currents, and θ is the flux angle of the controller.

As shown in Fig. 1, this control system does not require the detection values from the speed or position sensors. The flux-axis angular speed is estimated from the dq-axis voltages and the dq-axis currents. In addition, $\hat{\omega}$ is an instantaneous value which implies that if the motor current or motor voltage changed rapidly, a large error between the real value and calculated value might occur, leading to the instability of the system. In the flux-axis angular speed estimation in this paper, LPF is required to prevent the recursive computation.

A decoupling control is used in this system to remove the dq-axis voltage interference factors by feed-forward control. The d-axis voltage command v_d is calculated from the output of the d-axis current PI output v_d^*, the electrical angular speed $\hat{\omega}_r$, the stator inductance L_s, and the q-axis current i_q,

$$v_d = v_d^* - \hat{\omega}\rho(L_1 + M)i_q \tag{1}$$

The q-axis voltage command v_q is calculated from the output of q-axis current PI v_q^*, the secondary magnetic flux ϕ_{2d}, the d-axis current i_d, the leakage coefficient ρ, L_s and ω_{re},

$$v_q = v_q^* + \hat{\omega}(\rho\phi_{2d}\frac{M}{L_2} + L_1 i_d) \tag{2}$$

where ρ is defined as $\rho = 1 - M^2 / (L_1 L_2)$.

The secondary magnetic flux is calculated from the mutual inductance M, the rotor resistance R_2, the rotor inductance L_2 and i_d,

$$\phi_{2d} = i_d \frac{MR_2}{L_2} \times \frac{L_2}{L_2 s + R_2} \tag{3}$$

where s is the differential operator.

The slip angular speed is calculated from i_q, i_d, L_2 and R_2,

$$\omega_s = \frac{i_q}{i_d \dfrac{L_2}{R_2}} \tag{4}$$

B. Principle for Flux Axis Angular Velocity Estimation Method

The d-axis induced voltage e_d of the induction motor is controlled to zero. Hence, the flux-axis angular speed ω is calculated from the q-axis induced voltage e_q and the secondary d-axis flux ϕ_{2d} as:

$$\hat{\omega} = \frac{e_q}{\phi_{2d}} \tag{7}$$

Fig. 2 shows the induced voltage vector in dq-frame. Note that L_σ is the leakage inductance, R_1 is the primary resistance, and s is the differential operator. As shown in Fig. 2(b), the secondary d-axis flux ϕ_{2d} aligns with the d-axis when the induced voltage vector aligns to q-axis. In other words, if the secondary d-axis flux ϕ_{2d} is leading or lagging to the d-axis as shown in Fig. 2(a) and (c), the induced voltage vector includes the d-axis component. In these case, the flux axis angular speed cannot be calculated by (7). Instead, the flux-axis angular speed is estimated by using the dq-axis induced voltage and the compensation gain k_{pem} as:

$$\hat{\omega} = \frac{e_q}{\phi_{2d}} - k_{pem} e_d \tag{8}$$

Note that the definition of the unit of k_{pem} is (rad/s)/V.

The estimated induced voltage e_d and e_q are given by (9) and (10),

$$\hat{e}_d = v_d - (R_1 + L_\sigma \frac{d}{dt})i_d + \hat{\omega} L_\sigma i_q \tag{9}$$

$$\hat{e}_q = v_q - (R_1 + L_\sigma \frac{d}{dt})i_q - \hat{\omega} L_\sigma i_d \tag{10}$$

where L_σ is leakage inductance.

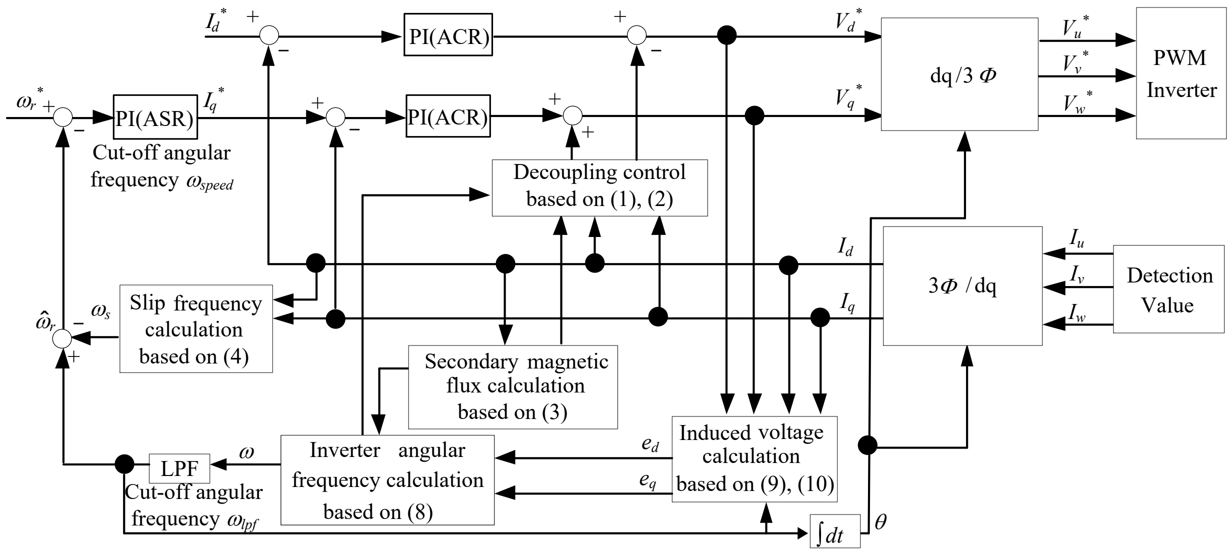

Fig. 1. Block diagram of flux-axis angular speed estimation.

III. Block Diagram of Flux Axis Angular Speed Estimation

Fig. 3 shows the analysis model of the flux-axis angular speed estimation with LPF. The closed-loop transfer function of the d-axis induced voltage is expressed by (11).

$$\frac{\hat{\omega}}{e_{\mathrm{d}}*}=\frac{\dfrac{k_{pem}}{1+k_{pem}L_{\sigma}i_{\mathrm{q}}}}{1+s\dfrac{1}{\omega_{lpf}\,(1+k_{pem}L_{\sigma}i_{\mathrm{q}})}} \tag{11}$$

Besides, the relationship between e_d^* and $\hat{e}_d$ as follows,

$$\frac{\hat{e}_d}{e_{\mathrm{d}}*}=\frac{\dfrac{k_{pem}L_{\sigma}i_{\mathrm{q}}}{1+k_{pem}L_{\sigma}i_{\mathrm{q}}}}{1+s\dfrac{1}{\omega_{lpf}\,(1+k_{pem}L_{\sigma}i_{\mathrm{q}})}} \tag{12}$$

According to (12), the steady-state error e_{derror} of the d-axis induced voltage is calculated by (13).

$$e_{derror}=1-\frac{k_{pem}L_{\sigma}i_{\mathrm{q}}}{1+k_{pem}L_{\sigma}i_{\mathrm{q}}} \tag{13}$$

The compensation gain k_{pem} is calculated from (13) as,

$$k_{pem}=\frac{1-e_{derror}}{L_{\sigma}i_{\mathrm{q}}\,(e_{derror}-1)} \tag{14}$$

However, according to Fig.3, the d-axis induced voltage should be calculated with the disturbance parts as,

$$\hat{e}_d=\frac{\dfrac{1}{1+k_{pem}L_{\sigma}i_{\mathrm{q}}}}{1+s\dfrac{1}{\omega_{lpf}\,(1+k_{pem}L_{\sigma}i_{\mathrm{q}})}}\left\{L_{\sigma}i_{\mathrm{q}}\frac{e_q}{\phi_{2d}}+(v_d-R_1 i_d)\right\} \tag{15}$$

According to (12) and (15), the time constant T_{model} and cut-off angular frequency ω_{model} of the designed model shown in Fig. 3 is calculated by (16).

$$T_{model}=\frac{1}{\omega_{model}}=\frac{1}{\omega_{lpf}\,(1+k_{pem}L_{\sigma}i_{\mathrm{q}})} \tag{16}$$

where the cut-off angular frequency of LPF ω_{lpf} is calculated by (17).

$$\omega_{lpf}=\frac{\omega_{model}}{(1+k_{pem}L_{\sigma}i_{\mathrm{q}})} \tag{17}$$

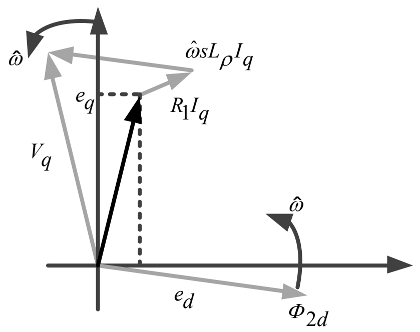

(a) ϕ_{2d} lagging behind d-axis.

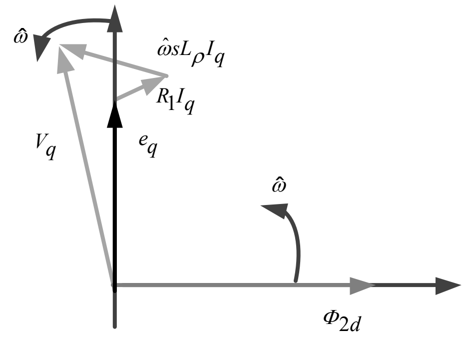

(b) ϕ_{2d} matching to d-axis.

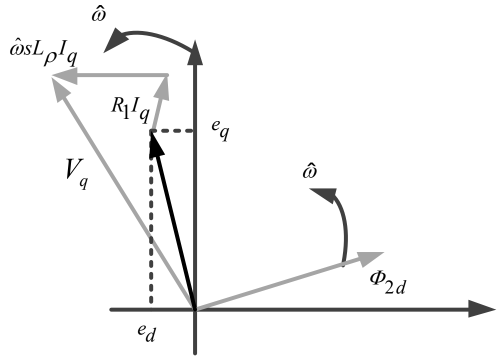

(c) ϕ_{2d} leading to d-axis.

Fig. 2. Induced voltage vector in dq-frame.

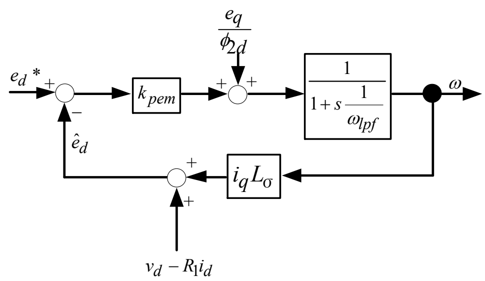

Fig. 3. Block diagram of flux axis angular speed estimation.

Fig. 4 shows the design flowchart for the flux axis angular speed estimation block. Firstly, the steady-state error and the cut-off angular frequency of speed controller is decided. Note that, $\hat{e}_d$ should be close to zero. However, it is difficult to obtain the zero of $\hat{e}_d$ because the steady-state error remains by P control as shown in Fig. 3. Besides, the cut-off angular frequency of the speed controller should be calculated from the motor parameter. Next, the k_{pem} is calculated by (14). Then, the cut-off angular frequency of the designed d-axis induced voltage model ω_{model} should be decided. The motor will be uncontrollable when ω_{model} is lower than ω_{ASR} because the designed model interferes the motor speed control. On the other hand, if the ω_{model} is high, the convergence time of the d-axis induced voltage is long. As the result, the convergence time of motor speed is long when a torque is given. Then, ω_{model} should be decreased. As the result, ω_{lpf} is calculated by (17).

Table I. Induction motor parameters.

Quantity	Symbol	Value
Poles paris	P_f	2
Rated power	P	3.7 kW
Rated voltage	Vn	188 V
Rated current	A_n	18 A
Primary resistance	R_1	0.414 Ω
Secondary resistance	R_2	0.423 Ω
Primary leakage inductance	L_1	34.54 mH
Secondary leakage inductance	L_2	34.54 mH
leakage inductance	L_σ	1.24 mH
Mutual inductance	M	34.3 mH
Moment of inertia	J	0.0163 kg･N
Rated speed	ω_n	1500 rpm

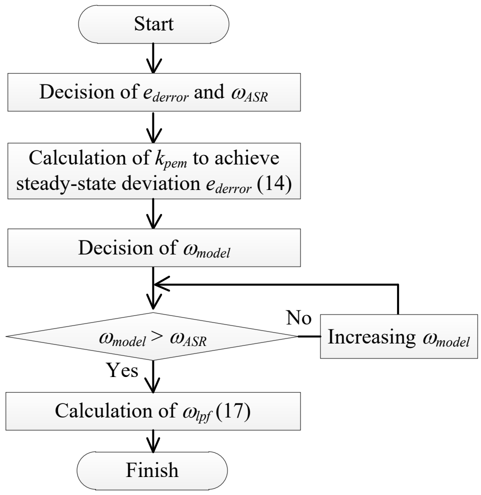

Fig. 4 Design flowchart for compensation gain k_{pem} and cut-off angular frequency of LPF ω_{lpf}

IV. Simulation Results

Table I lists the induction motor parameters. In order to confirm the validity of the proposed sensor-less vector FOC, a 3.7 kW prototype of the general-purpose induction motor was tested. Note that, the cut-off frequencies of the current and speed regulations are 600 Hz and 30 Hz (188.4 rad/s), respectively, whereas both the sampling frequency and switching frequency are 20 kHz.

Fig. 5 shows the simulation result with the speed sensor-less FOC using the proposed flux-axis angular speed estimation. As shown in Fig. 5, the speed command starts to increase after 0.8 second with no load, then, the rated load torque step is applied after 1.5 second. At all times, the actual speed follows the command value. As the result, when a torque step is applied to the motor, a speed error occurs. Note that the estimated value agrees with the actual value of the d-axis induced voltage.

Fig. 6 shows the simulation result with the speed sensor-less FOC using the proposed design model of flux-axis angular speed estimation. As shown in Fig. 6(a), 100% of the motor torque step is applied after 1.5 second. As the result, when a torque step is applied to the motor, the q-axis current ripple and motor speed ripple occurs. When the compensation gain k_{pem} is set as 8.0 p.u. and ω_{lpf} is set as 200 rad/s, the convergence time of the motor speed is the shortest. Meanwhile, when k_{pem} is set as 1.0 p.u. and ω_{lpf} is set as 1000 rad/s, the convergence time of the motor speed is the longest. As shown in Fig. 6(b), the same condition is applied as Fig. 6(a). As the result, when the LPF cut-off angular frequency ω_{lpf} is set as 107 rad/s, the motor is uncontrollable. Meanwhile, when ω_{lpf} is set as 1000 rad/s, the convergence time of the motor speed is the longest. The relation between k_{pem}, ω_{lpf}, convergence time of the d-axis induced voltage follow the designed model, (14) and (17).

Fig. 7 shows the value and the error rate of the steady-state error of the d-axis voltage against the compensation gain k_{pem}. The compensation gain k_{pem} are varied from 1.0 p.u. to 15.0 p.u.. That is calculated form (15). As the result, the standard deviation of the d-axis voltage from the simulation almost follows the estimated value. In particular, the maximum error between the simulation and estimated results of the time constant of the flux-axis

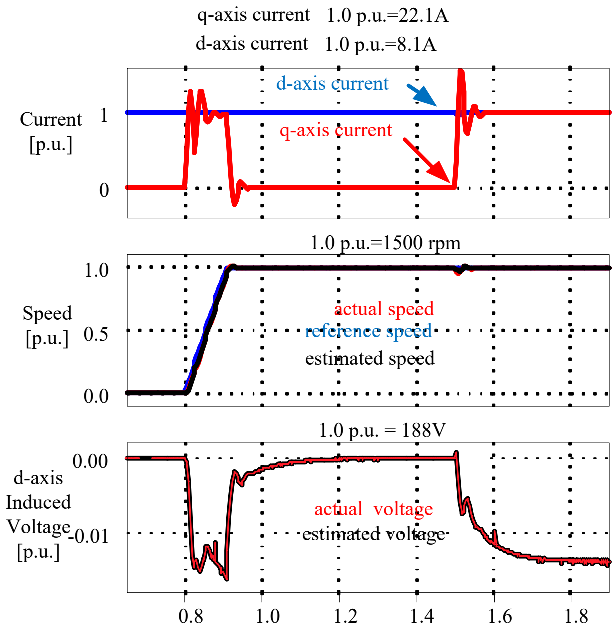

Fig. 5. Speed control simulation result with the sensor-less FOC.

angular speed is 2.3% at the compensation gain k_{pem} of 3.0 p.u. due to the parameter mismatch of the v_d, e_q, i_q, as shown in Fig.3. These results confirm the validation of the proposed design method for the flux-axis angular speed estimation. Moreover, the effects of k_{pem} on the d-axis induced voltage regulation can be observed from Fig. 7 as follows; if the compensation gain k_{pem} is low, the standard deviation of the d-axis voltage is high.

Fig. 8 shows the relation between the time constant and cut-off frequency obtained from simulation and estimated results. As shown in Fig. 8, the d-axis induced voltage command e_d^* is set as a step change from 0 p.u. to 0.02 p.u. in the closed-loop. Note that the time constant of the flux axis angular speed obtained from the simulation almost follows the estimated value. In particular, the maximum error between the simulation and estimated results of the time constant of the flux-axis angular speed is 3.7% at the LPF cut-off angular frequency ω_{lpf} of 200 rad/s. These results confirm the validation of the proposed design method for the flux-axis angular speed estimation.

Moreover, the effects of LPF on the d-axis induced voltage regulation can be observed from Fig. 8 as follows; if the cut-off angular frequency of LPF is high, the time constant becomes high and the convergence time becomes long. In addition, if the compensation gain k_{pem} is high, the time constant also becomes high and the convergence time of the d-axis induced voltage also becomes long.

Fig. 9 shows the relation between the convergence time of the motor speed, the cut-off angular frequency of LPF ω_{lpf} and the compensation gain k_{pem}. If the cut-off angular frequency of the LPF is high, the convergence time of the motor speed is long. In addition, if the compensation gain k_{pem} is high, the convergence time also becomes long. Note that these characteristics the result shown in Fig. 8.

V. EXPERIMENTAL RESULTS

The effectiveness of the proposed design method of the flux-axis angular-speed estimation using the induced voltage is verified. In the experiment, a three-phase induction motor (MVK8115A-R, Fuji Electric Co., Ltd) with the parameters shown in Table 1 is used as the test motor. The motor is driven by the proposed design method. The load torque is varied by controlling of the load motor. The cut-off frequencies of the current and speed regulations are 600 Hz and 30 Hz, respectively, whereas both the sampling frequency and the switching frequency are 20 kHz, which are the same conditions as simulation.

Fig. 10 shows the experimental waveforms of the phase current and the line-to-line voltage with the conventional vector control and the proposed sensor-less FOC, respectively.

Fig. 11 shows the experimental waveforms of the dq-axis currents, the detected and estimated motor speeds. In any case, the detected speed follows the speed command of 1500 rpm. In the conventional vector control, the motor speed does not contain any ripple. In contrast, as shown in Fig. 11 (b) and (d), when the compensation gain k_{pem} is set as 2.0 p.u., a current ripple occurs when the motor is 0 rpm. That is caused by the d-axis induced voltage calculation in (9) which is using the q-axis current. In addition, when the motor does not have any load, the detection relative error of the q-axis current is big. Furthermore, if k_{pem} is high, the calculation relative error of the flux-axis angular speed is big. This is because the d-axis induced voltage calculation uses the q-axis current. When the compensation gain k_{pem} is set as 2.0 p.u. and ω_{lpf} is set as 1000 rad/s as shown in Fig. 11(d), a speed ripple occurs at beginning of the motor acceleration because the time constant of the d-axis voltage is low, which follows the (17).

Fig. 12 shows the experimental waveforms of the dq-axis current, the detected speed when the torque step is applied. In any case, the speed error occurs when the torque step is applied to the induction motor. In the conventional vector control, the maximum speed error speed is 3%, and the convergence time is 100 ms. In contrast, in the proposed speed sensor-less FOC, the speed ripple of 8% occurs and the convergence time is longer than that of the conventional vector control. In particular, when the compensation gain k_{pem} is set as 2.0 p.u. and ω_{lpf} is set as 200 rad/s, the convergence time is 430 ms, which is 62.3% of that when the compensation gain k_{pem} is set as 2.0 p.u. and ω_{lpf} is set as 1000 rad/s. As the result, if the time constant of the d-axis induced voltage is low as shown

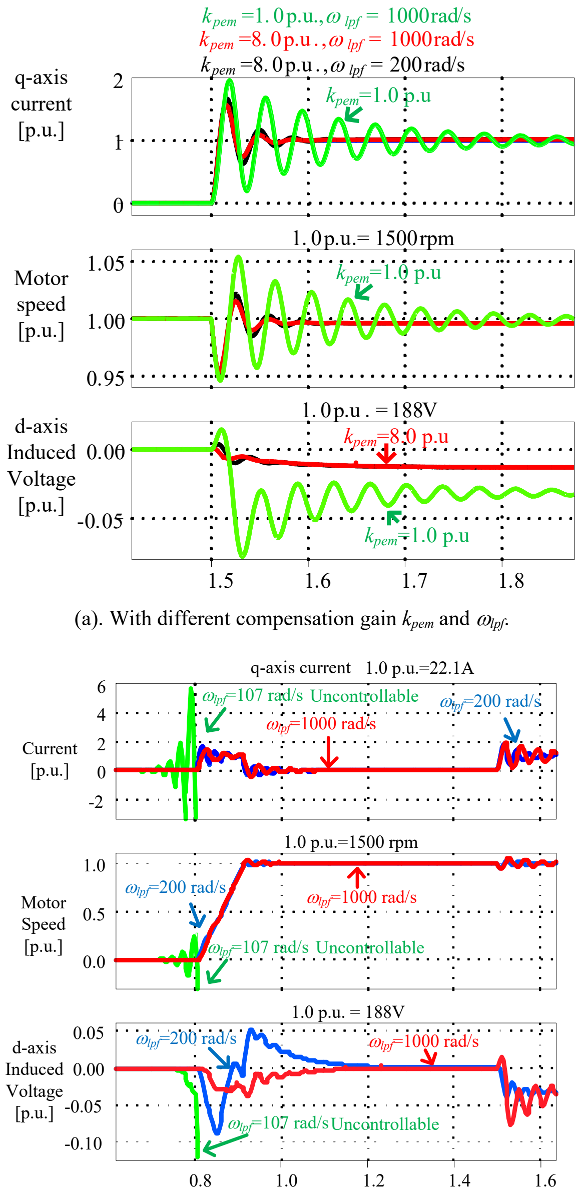

Fig. 6. Speed control simulation result with proposed sensor-less FOC with different design parameters.

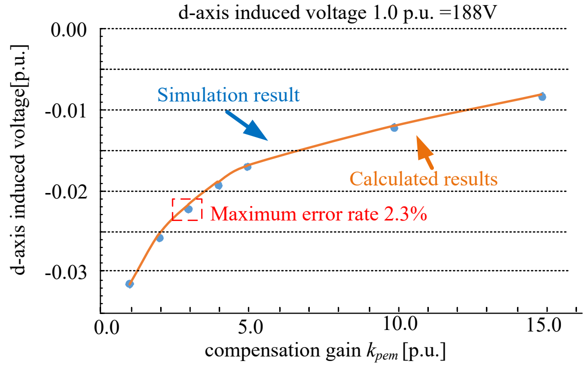

Fig. 7. Relation between compensation gain k_{pem} and standard deviation from simulation and estimated results

in (19), the convergence time of the d-axis induced voltage is long. In other words, the motor speed convergence time becomes long.

Fig. 13 shows the relation among the experimental results of the motor speed convergence time, the compensational gain k_{pem} and the LPF cut-off angular frequency ω_{lpf}. When a torque step of 100% is applied, the convergence time of the motor speed is 1.6 s as the worst case with the compensation gain k_{pem} set as 2.0 p.u. and the cut-off angular frequency set as 400 rad/s. However, if the compensation gain k_{pem} is set as 2.0 p.u. and the cut-off angular frequency is set as 400 rad/s, the convergence time of the motor speed is 0.43 s as the best case, which is reduced by 73.1% compared to the worst case. The effects of LPF in the flux-axis angular speed ω calculation can be observed from Fig. 13 as follows; if the cut-off angular frequency of the LPF is high, the motor speed convergence time is long. In addition, if the compensation gain k_{pem} is high, the motor speed convergence time is long, which follows (19) and the simulation result shown in Fig. 9. The cause of the large convergence time error between simulation result in Fig. 9 and experiment result in Fig.13 is that the real motor parameters is not as same as the design parameters in PI current controller and PI speed controller.

VI. Conclusion

This paper proposed the design method of the flux-axis angular speed estimation using the induced voltage for IM drive systems. LPF was required in the flux-axis angular speed estimation to stabilize the d-axis induced voltage regulation. The effects of this LPF on the d-axis induced voltage regulation was evaluated. In particular, the maximum error between the simulation and estimated results of the time constant of the flux-axis angular speed was 3.7% when the cut-off angular frequency of LPF ω_{lpf} as 200 rad/s.

As the experimental results, LPF highly affected the flux axis angler speed ω. Besides, when the torque step of 100% was applied, the convergence time of the motor speed was 1.6 sec. as the worst case with the compensation gain k_{pem} set as 1.0 p.u. and the cut-off angular frequency set as 1000 rad/s. However, if the compensation gain k_{pem} was set as 2.0 p.u. and the cut-off angular frequency ω_{lpf} was set as 400 rad/s, the convergence time of the motor speed was 0.43 sec. as the best case, which was reduced by 73.1 % compared to the worst case.

As the conclusion, the cut-off angular frequency of LPF ω_{lpf} highly affected the flux-axis angular-speed. The relation among the flux-axis angular-speed, ω_{lpf} and the compensation gain k_{pem} was as follows; if the ω_{lpf} was high, the time constant of flux-axis angular-speed was high and the convergence time of motor speed was long. Moreover, if the compensation gain k_{pem} was high, the time constant of flux-axis angular-speed was high and the convergence time of motor speed was long, which followed the model and equation shown in this paper. Note that if the convergence time of the motor speed was long, the ripple of the motor speed might occur. In the future work, the design value of k_{pem} and the cut-off angular frequency of LPF ω_{lpf} should be clarified by calculation.

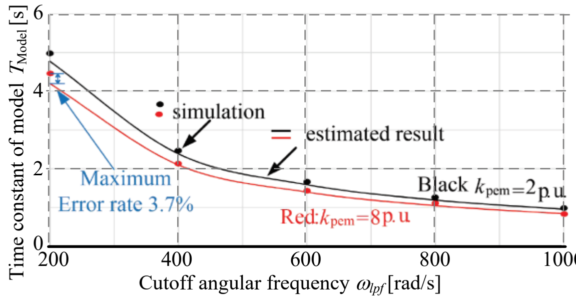

Fig. 8. Relation between time constant and cutoff frequency obtained from simulation and estimated results.

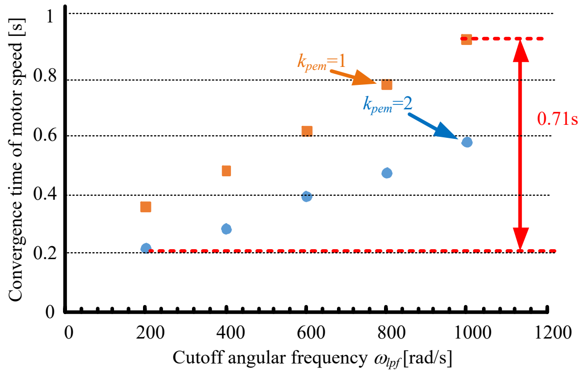

Fig. 9. Relation between time constant and cutoff frequency obtained from simulation and estimated results.

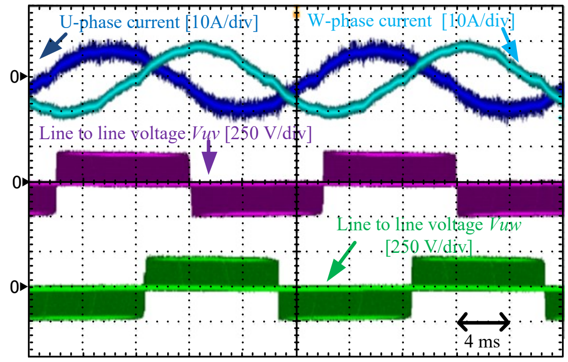

(a) With conventional vector control.

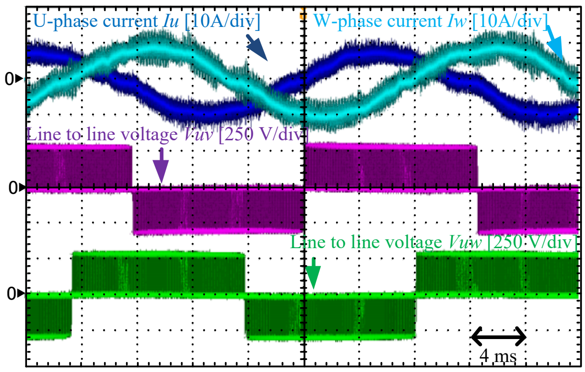

(b) With the speed sensor-less FOC(k_{pem} = 1.0 p.u., ω_{lpf}=200 rad/s).

Fig. 10. Experimental waveforms of line-to-line voltages and phase currents.

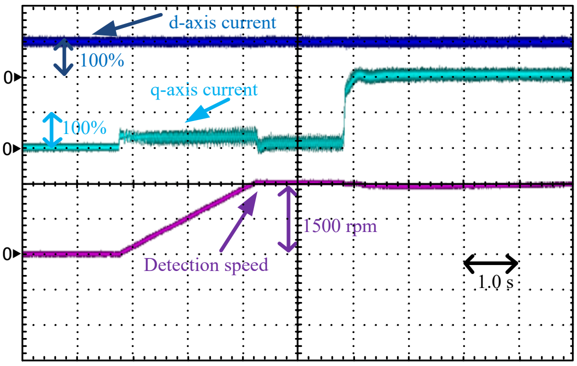

(a) With conventional vector control.

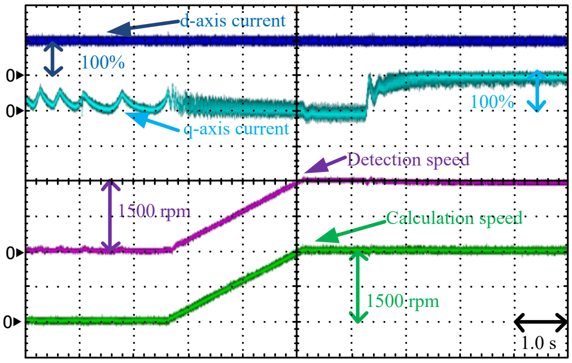

(b)With speed sensor-less FOC (k_{pem} = 2.0 p.u., ω_{lpf}=200 rad/s).

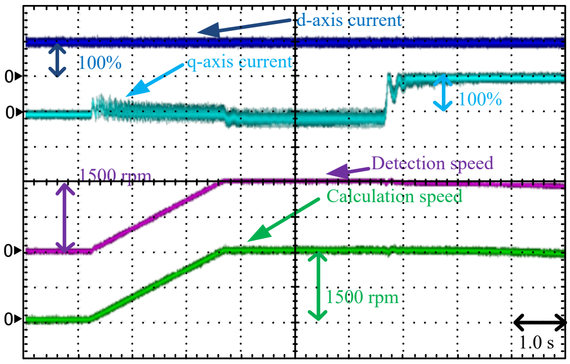

(c) Convergence time of motor speed increase by k_{pem} with speed sensor-less FOC (k_{pem} = 1.0 p.u., ω_{lpf}=200 rad/s)..

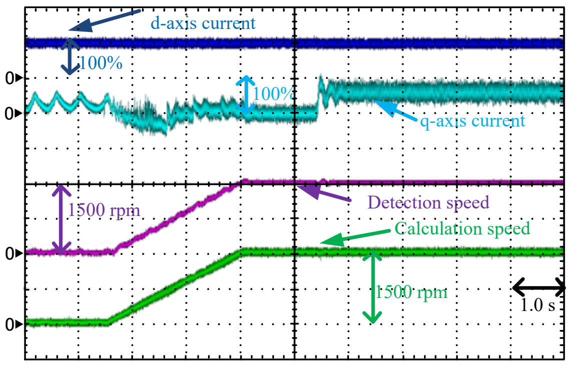

(d) Convergence time of motor speed increase by ω_{lpf} with speed sensor-less FOC (k_{pem} = 2.0 p.u., ω_{lpf}=1000 rad/s).

Fig. 11. Experimental waveforms of dq-axis current, detection speed and calculation speed.

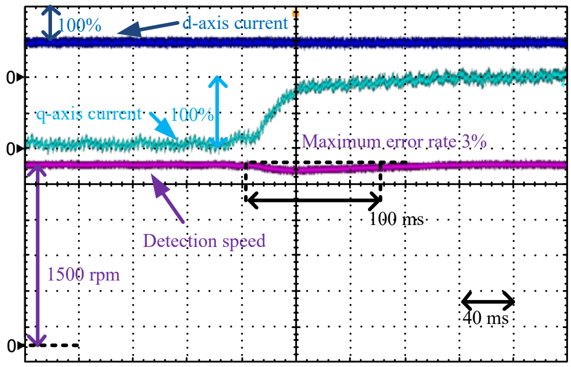

(a)With conventional vector control.

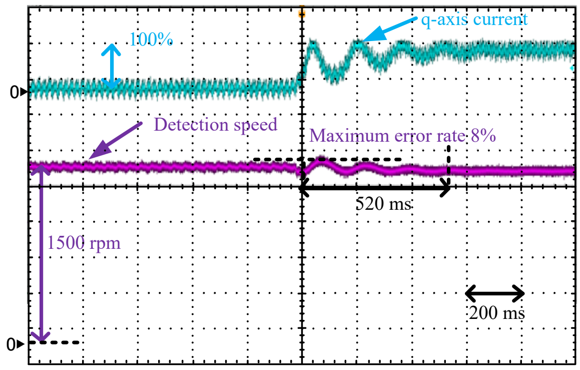

(b)With speed sensor-less FOC (k_{pem} = 1.0 p.u., ω_{lpf}=200 rad/s).

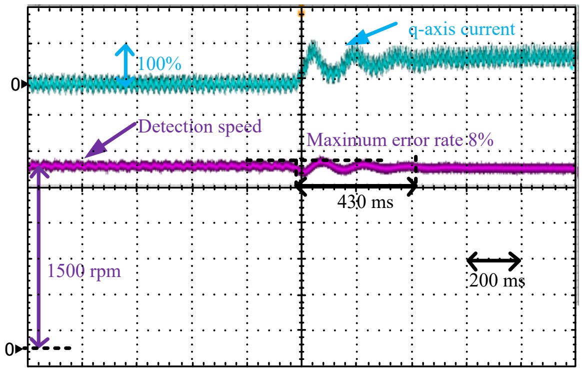

(c) Convergence time of motor speed increase by k_{pem} with speed sensor-less FOC (k_{pem} = 2.0 p.u., ω_{lpf}=200 rad/s).

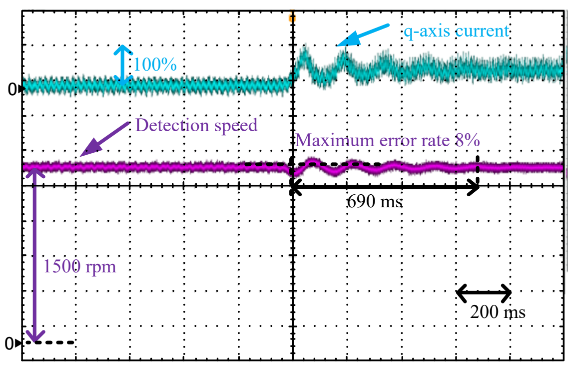

(d) Convergence time of motor speed increase by ω_{lpf} with speed sensor-less FOC (k_{pem} = 2.0 p.u., ω_{lpf}=1000 rad/s).

Fig. 12. Experimental waveforms of speed when a torque was given.

REFERENCES

[1] J. Itoh, N. Nomura, H. Ohsawa: “A comparison between V/f control and position-sensorless vector control for the permanent magnet synchronous motor”, in Proc. Power Conversion Conf., Vol. 3, pp. 1310-1315, (2002)

[2] J. Itoh, T. Toi, M. Kato: "Maximum Torque per Ampere Control Using Hill Climbing Method Without Motor Parameters Based on V/f Control", EPE'16, Vol., No. DS3d-Topic 4-0283, pp. (2016)

[3] S. Fot, A. Testa, S. De Caro, T. Scimone, G. Scelba and G. Scarcella, "Rotor Time Constant Identification on Sensorless Induction Motor Drives by low Frequency Signal Injection," 2018 IEEE 9th International Symposium on Sensorless Control for Electrical Drives (SLED), Helsinki, 2018, pp. 150-155.

[4] Takumi Kurosawa, and Yasutaka Fujimoto,"Torque Sensorless Control for an Electric Power Assisted Bicycle with Instantaneous Pedaling Torque Estimation",IEEJ J. Industry Applications, vol.6, no.2, pp.124-129, 2017.

[5] Ufot Ufot Ekong, Mamiko Inamori, and Masayuki Morimoto"Instantaneous Vector Control of Four Switch Three Phase Inverter Fed Induction Motor Drive,"IEEJ J. Industry Applications, vol. 6, no. 6, pp. 429-434, 2017.

[6] H. Tajima, Y. Matsumoto, H. Umida,"Speed Sensorless Vector Control Method for an Industrial Drive System"IEEJ,Vol. 116 No. 11(1996).

[7] H. Tajima, Y. Hori, "Speed-sensorless field-orientation control of the induction machine". IEEE Transactions on Industry Applications, 1993, 29(1): 175 180.

[8] T. Hoshino, J. Itoh. "Output Voltage Correction for a Voltage Source Type Inverter of an Induction Motor Drive." IEEE Transactions on Power Electronics. 2010, Vol.25, No.9, p.2440.

[9] M. Bobrov and G. Tutaev, "Flux Estimation Algorithms for Double-Fed Induction Motor Drive Field-Oriented Control," 2018 X International Conference on Electrical Power Drive Systems (ICEPDS), Novocherkassk, 2018, pp. 1-6.

[10] Shrinathan Esakimuthu Pandarakone, Yukio Mizuno, and Hisahide Nakamura"Online Slight Inter-Turn Short-Circuit Fault Diagnosis Using the Distortion Ratio of Load Current in a Low-Voltage Induction Motor,"IEEJ J. Industry Applications, vol. 7, no. 6, pp. 473-478, 2018.

[11] Y. Cui, W. Huang, N. Su and F. Bu, "Adaptive Full-Order Observer for Induction Motor Based on Bilinear Transformation Method," 2018 21st International Conference on Electrical Machines and Systems (ICEMS), Jeju, 2018, pp. 1649-165

[12] K. H. Park, C. Moon, K. H. Nam, M. K. Jung and Y. A. Kwon, "State observer with parameter estimation for sensorless induction motor," SICE Annual Conference 2011, Tokyo, 2011, pp. 2967-2970.

[13] S. J. Rind, A. Amjad and M. Jamil, "Rotor Flux MRAS based Speed Sensorless Indirect Field Oriented Control of Induction Motor Drive for Electric and Hybrid Electric Vehicles," 2018 53rd International Universities Power Engineering Conference (UPEC), Glasgow, 2018, pp. 1-6.

[14] Vonkomer, J.; Zalman, M., "Induction motor sensorless vector control for very wide speed range of operation," IEEE, 2011 12th International, pp.437,442, 25-28 May 2011

[15] M. Tsuji, S. Chen, K. Izumi, E. yamada, "A sensorless vector control system for induction motors using q-axis flux with stator resistance identification", IEEE Transactions on Industry Applications, vol. 48, pp. 185-194, 2001.

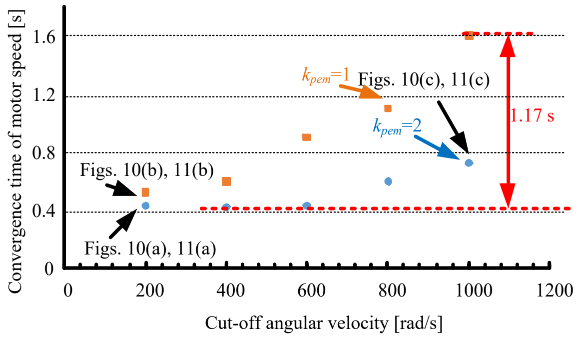

Fig. 13. Relation between time constant and cutoff frequency obtained from simulation and estimated results.

[16] J. Cao, G. Li, X. Qi, Q. Ye, Q. Zhang and Q. Wang, "Sensorless vector control system of induction motor by nonlinear full-order observer," 2016 IEEE 11th Conference on Industrial Electronics and Applications (ICIEA), Hefei, 2016, pp. 1959-1962.

[17] S. N. Agrawal and S. P. Muley, "MRAS based speed sensorless vector control of Induction motor," 2017 2nd International Conference on Communication and Electronics Systems (ICCES), Coimbatore, 2017, pp. 69-72

[18] M. T. Joy and J. Böeker, "Sensorless Control of Induction Motor Drives Using Additional Windings on the Stator," 2018 IEEE 9th International Symposium on Sensorless Control for Electrical Drives (SLED), Helsinki, 2018, pp. 162-167.

[19] D. FEREKA, M. ZERIKAT and A. BELAIDI, "MRAS Sensorless Speed Control of an Induction Motor Drive based on Fuzzy Sliding Mode Control," 2018 7th International Conference on Systems and Control (ICSC), Valencia, 2018, pp. 230-236.